Electronic Supplementary Material (ESI) for Dalton Transactions.

This journal is © The Royal Society of Chemistry 2022

SUPPLEMENTARY MATERIAL

Three layered cucurbit[6]uril-based metal-organic rotaxane networks functionalized by sulfonic groups for proton conduction

Ying Li,[a] Yan-Jun Xu,[a] Ming-Yue Fan,[a] Zhen-Jie Feng,[a] Jun-Jun Li,[a] Xue-Song Wu,*[a] Jing Sun,[a] Xin-Long Wang[a,b] and Zhong-Min Su*[a,b]

[a] Jilin Provincial Science and Technology Innovation Center of Optical Materials and Chemistry, School of Chemistry and Environmental Engineering, Changchun University of Science and Technology, Changchun, 130022, People's Republic of China.

[b] National & Local United Engineering Laboratory for Power Battery Institution, Northeast Normal University, Changchun, Jilin, 130024, People's Republic of China

*Corresponding Author E-mail: wxs@cust.edu.cn (X.-S. Wu); zmsu@nenu.edu.cn (Z.-M. Su).

Experimental Section

Materials and Physical Measurements.

$[PR63]^{2+}\cdot 2[NO_3]^-$, $[PR43]^{2+}\cdot 2[NO_3]^-$and CB[6] were synthesized according to references.[1,2] CB[6] was allowed to preassemble with C6N3 and C4N3 in water to form the pseudorotaxane ligands, i.e. $[PR63]^{2+}\cdot 2[NO_3]^-$ and $[PR43]^{2+}\cdot 2[NO_3]^-$. All other chemicals (analytical pure) were commercially purchased and used without any further purification. The formulae and visualized crystal structure of all compounds were obtained by single-crystal X-ray diffraction. The IR spectra were recorded using KBr pellets in the range of 4000–400 cm^{-1} on a Nicolet Magna 750 FTIR spectrometer. Thermogravimetric analysis (TGA) was performed on a EVO2G-TG-08 analyzer over the temperature 25–800 °C in a nitrogen-gas atmosphere with a heating rate of 10 °C min^{-1}. Powder X-ray diffraction (PXRD) spectra were measured on Rigaku Smart Lab with Cu-Kα (λ = 1.5418 Å) radiation in the range 5-50°.

X-ray Crystallographic Study.

All data collections were performed on a Bruker D8-Venture diffractometer with a Turbo X-ray Source (Cu Kα radiation, λ=1.5418Å for **CUST-711** and **CUST-713**, Mo Kα radiation, λ=0.71073Å for **CUST-712**). The data of crystals were collected at room temperature and the absorption correction was achieved using SADABS. The structure of crystals was solved by means of direct methods and refined by F2 full-matrix refinement using the SHELXTL package (SHELXTL-97) and Olex2 software packages. C-H and N-H were placed in geometrically calculated positions. Further details of the X-ray structural analysis of compounds are given in **Table 1**. The crystallographic data of **CUST-711**, **CUST-712** and **CUST-713** have been deposited in the Cambridge Crystallographic Data Center as supplementary publication with CCDC 2127144, 2127145 and 2127146.

Impedance analysis.

AC impedance tests were carried out on pressed pellets of finely ground powder samples. Samples for conductivity measurements were prepared by grinding the sample (~30mg) into a homogeneous powder with a mortar and pestle, added to a standard 5 mm die, and pressed at 1000 psi for 2 minutes. The proton conduction behaviors of materials were measured on Versa STAT 3 (Princeton Applied Research) electrochemical work station by alternating-current (AC) impedance measurements over frequency range of 1 Hz to 1 MHz at an amplitude of 500 mV and 0 mV DC rest voltage. The measurements were operated at temperatures (40 to 85℃), with different relative humidities (75% to 97% RH). The proton conductivity was calculated using the following equation the following equation $\sigma = L/(RA)$， where L and A are the thickness (cm) and cross-sectional area (cm^2) of the pellet respectively, and R, which was extracted from the impedance plots. The activation energy values were obtained from the slope of Arrhenius plots by least-squares fitting. ZView software was used to analyse the impedance data.

Table S1. Selected bond length (Å) for compounds.

CUST-711		CUST-712		CUST-713	
Cu(1)-O(1)[1]	1.9608(18)	Cu(1)-O(1)	1.973(2)	Cu(1)-O(1)[1]	1.953(3)
Cu(1)-O(3)	1.948(2)	Cu(1)-O(2)	1.975(3)	Cu(1)-O(2)	1.952(3)
Cu(1)-O(4)	1.998(2)	Cu(1)-O(5)[1]	1.977(3)	Cu(1)-N(1)	1.990(4)
Cu(1)-N(1)	2.009(3)	Cu(1)-N(1)	2.007(3)	Cu(1)-O(8)	1.940(4)
Cu(1)-O(14)	2.265(3)	Cu(1)-O(11)	2.366(3)	Cu(1)-O(6)[1]	2.545(4)
Cu(1)-O(12)[1]	2.841(3)	Cu(1)-O(15)	2.848(3)	Cu(1)-O(12)	2.706(4)

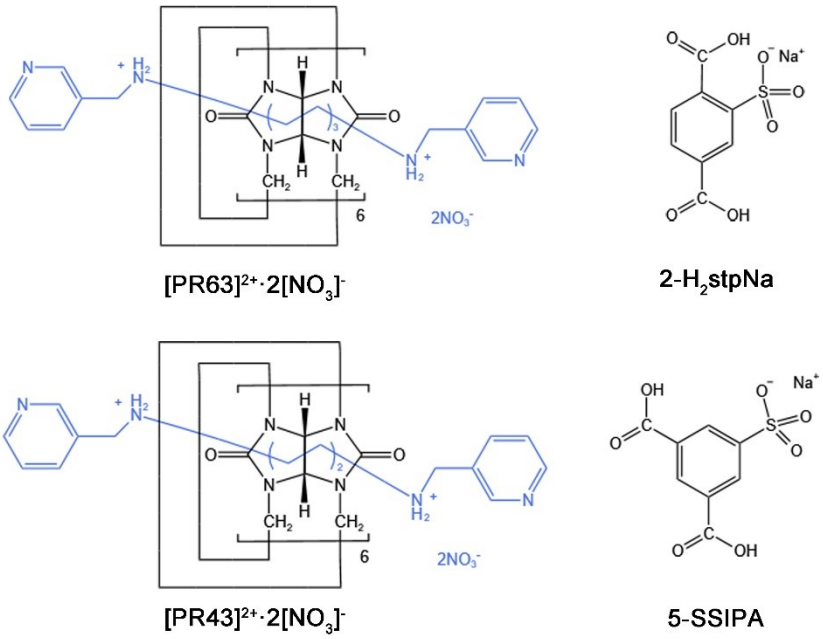

Fig. S1 The chemical structure formula of $[PR63]^{2+}\cdot 2[NO_3]^-$, $[PR43]^{2+}\cdot 2[NO_3]^-$, 2-$H_2$stpNa and 5-SSIPA.

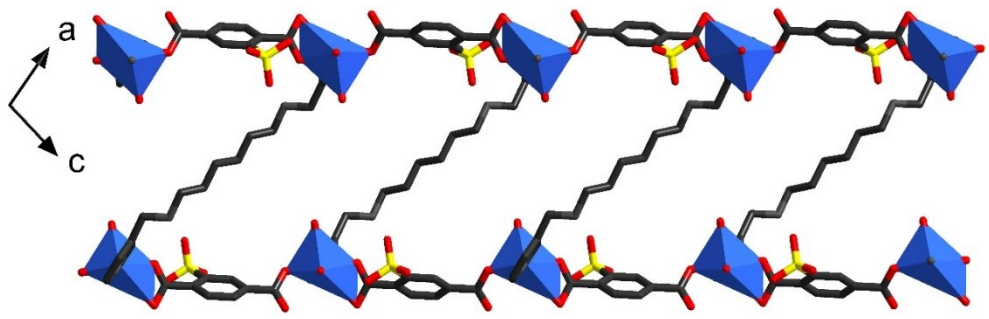

Fig. S2 Chemical view of pore channels of **CUST-711**.

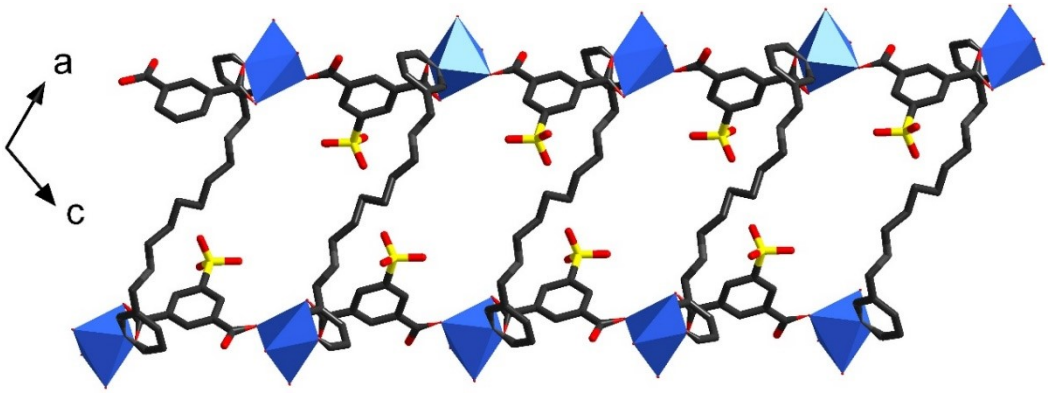

Fig. S3 Chemical view of pore channels of **CUST-712**.

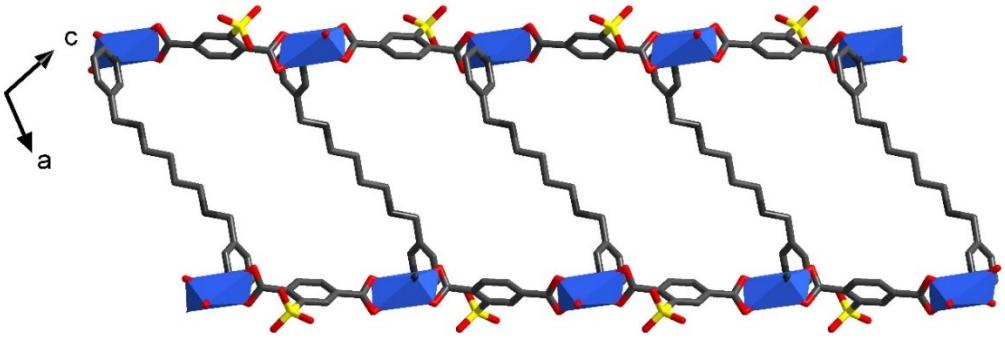

Fig. S4 Chemical view of pore channels of **CUST-713**.

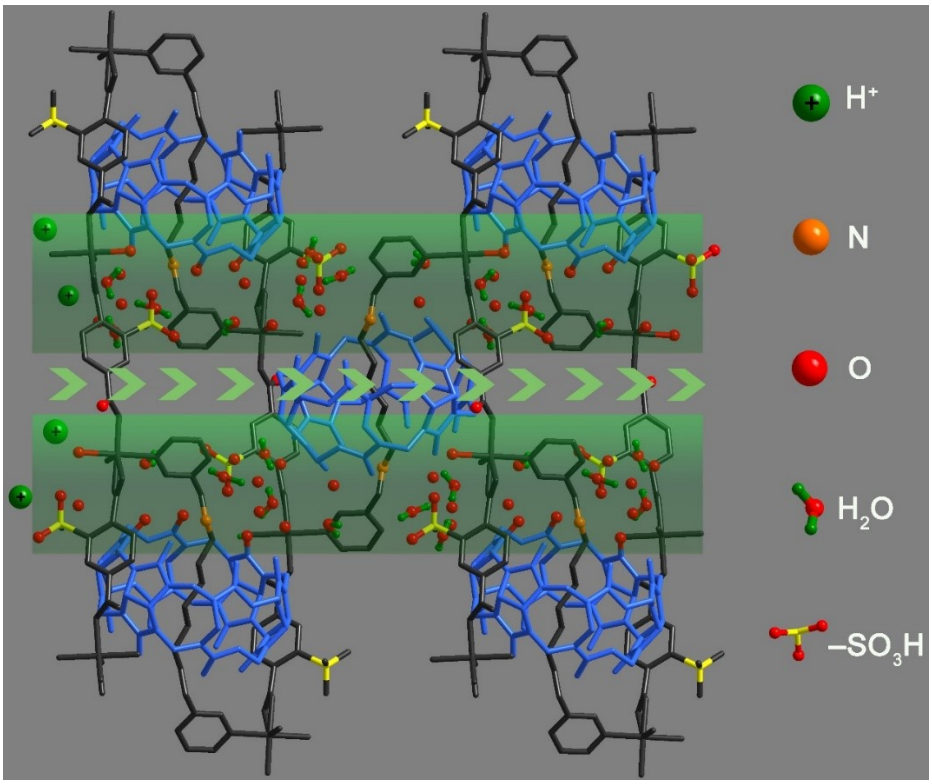

Fig. S5 Schematic of proton transfer in **CUST-712**.

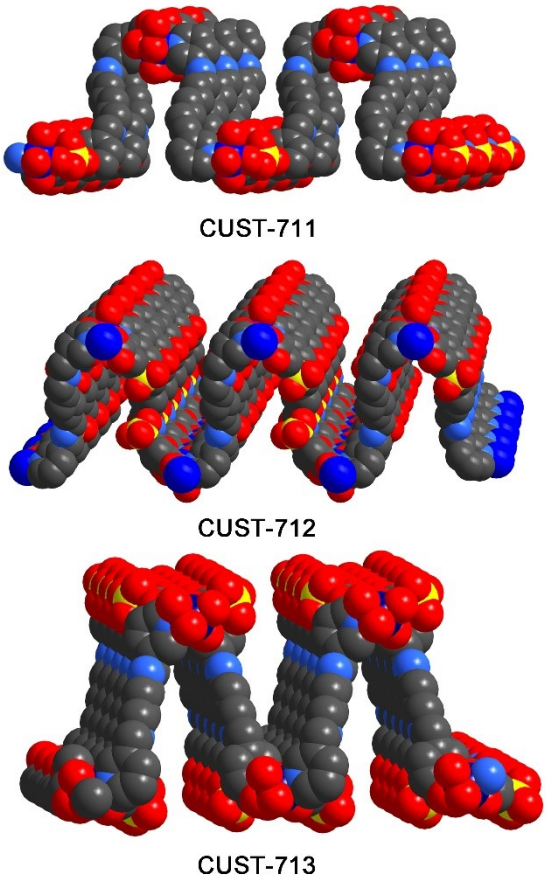

Fig. S6 Two-dimensional wave layer structure of three compounds in filled mode, CB[6]s are omitted for clear.

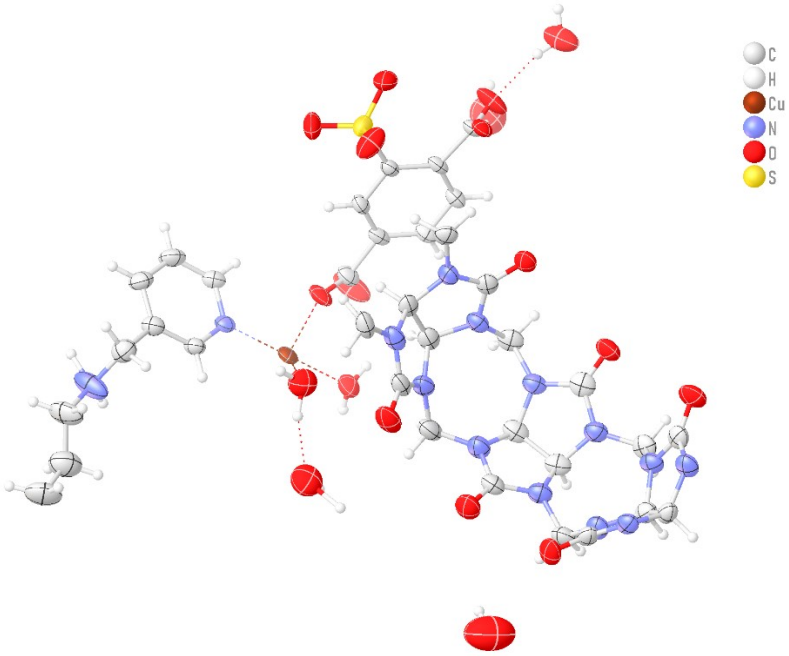

Fig. S7 ORTEP drawing of the asymmetric unit of **CUST-711**, probability.

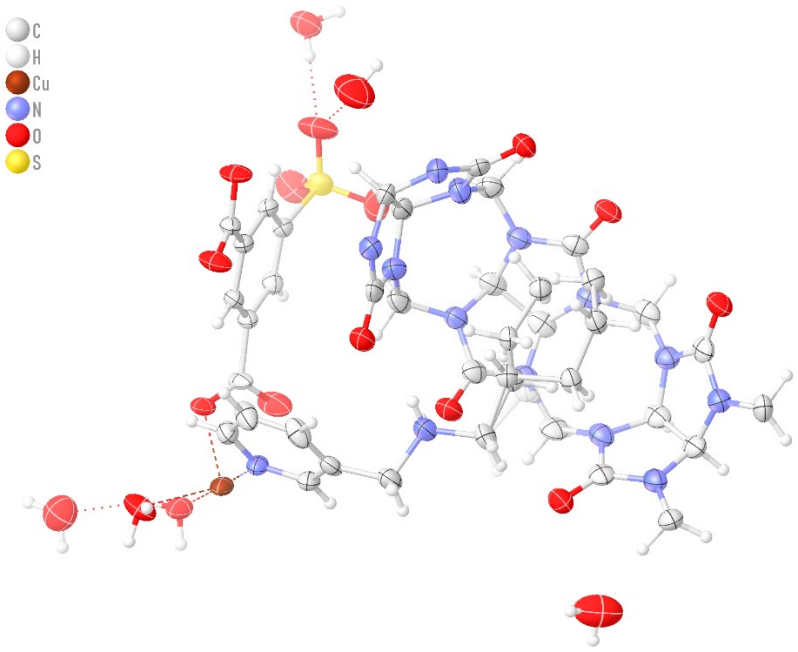

Fig. S8 ORTEP drawing of the asymmetric unit of **CUST-712**, probability.

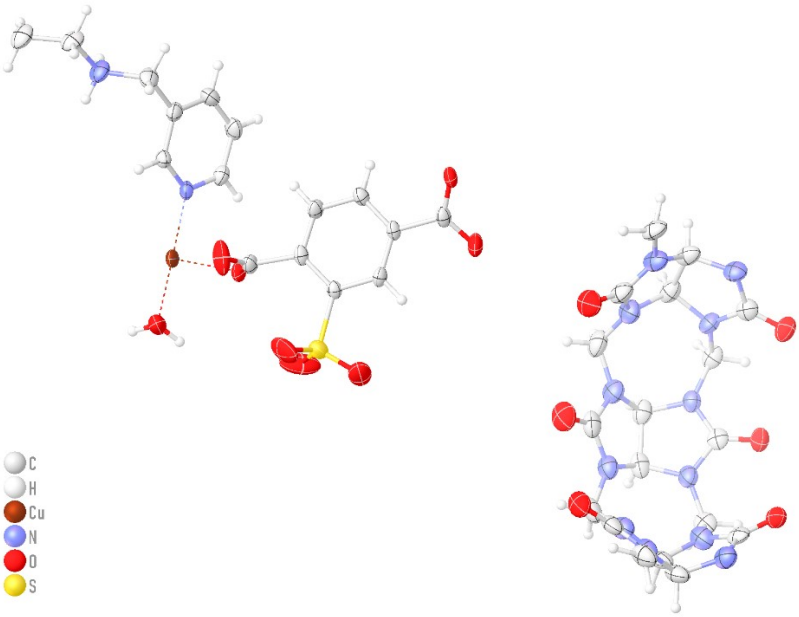

Fig. S9 ORTEP drawing of the asymmetric unit of **CUST-713**, probability.

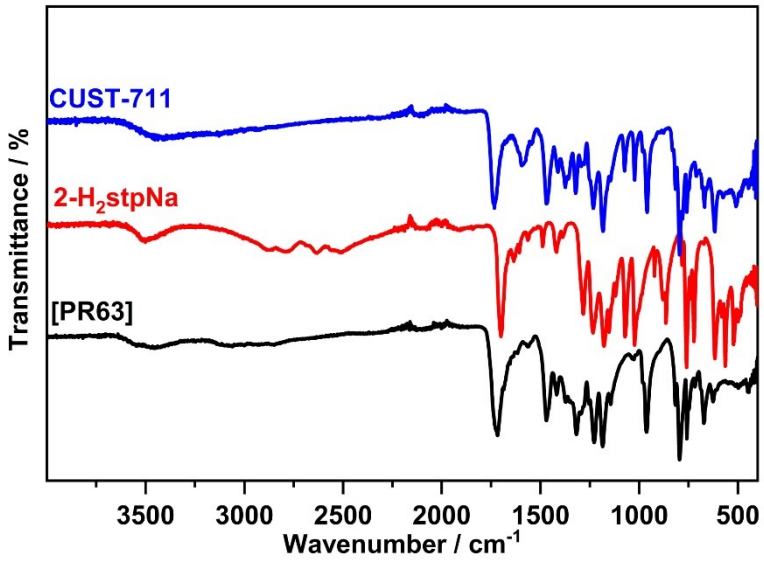

Fig. S10 Infrared absorption spectrum of 2-H_2stpNa, $[PR63]^{2+}\cdot 2[NO_3]^-$, **CUST-711**.

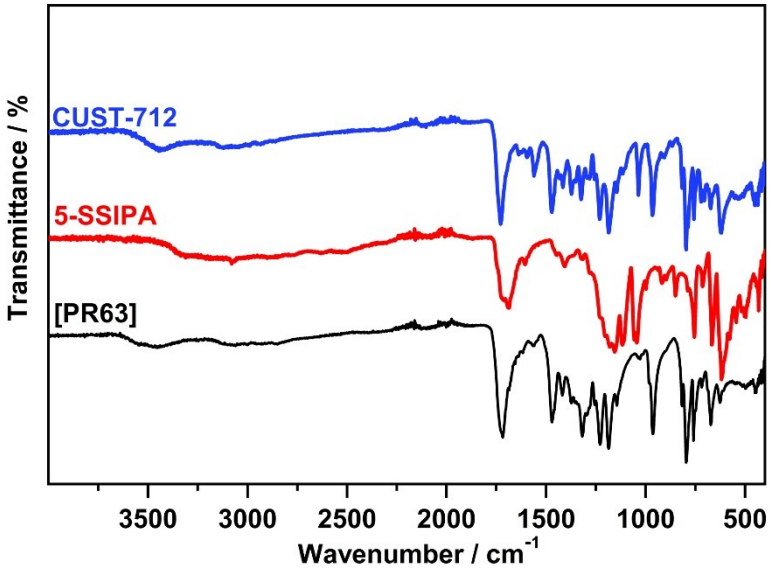

Fig. S11 Infrared absorption spectrum of 5-SSIPA, $[PR63]^{2+}\cdot 2[NO_3]^-$, **CUST-712**.

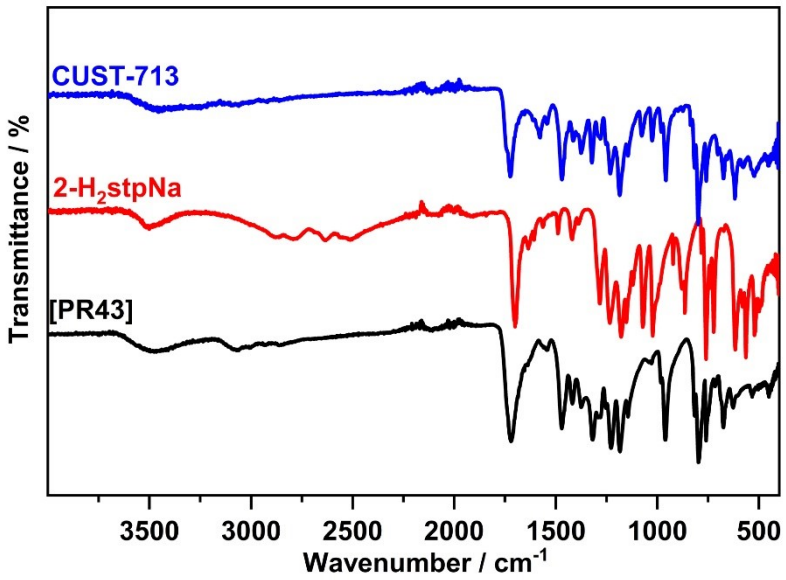

Fig. S12 Infrared absorption spectrum of 2-H_2stpNa, $[PR43]^{2+}\cdot 2[NO_3]^-$, **CUST-713**.

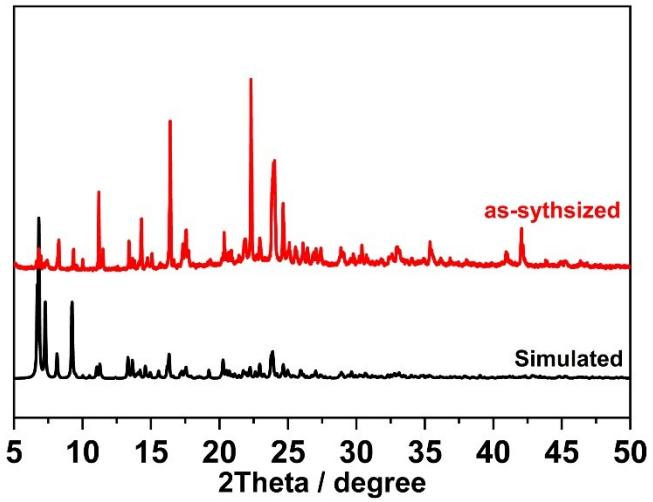

Fig. S13 Simulated and as-synthesized PXRD patterns of **CUST-711**.

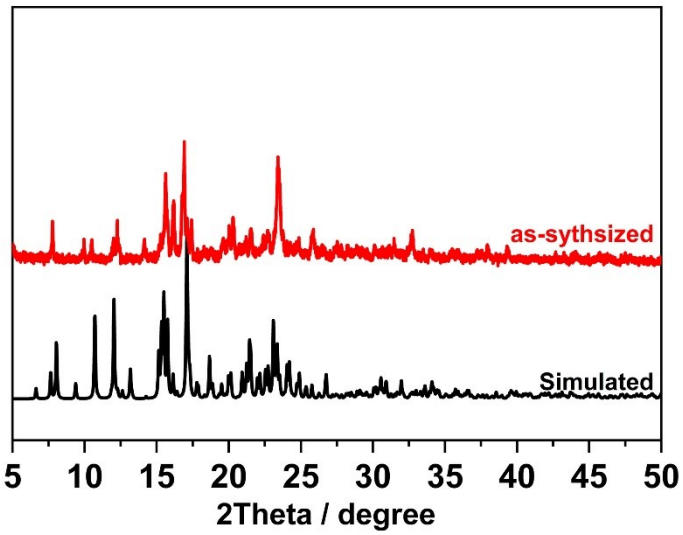

Fig. S14 Simulated and as-synthesized PXRD patterns of **CUST-712**.

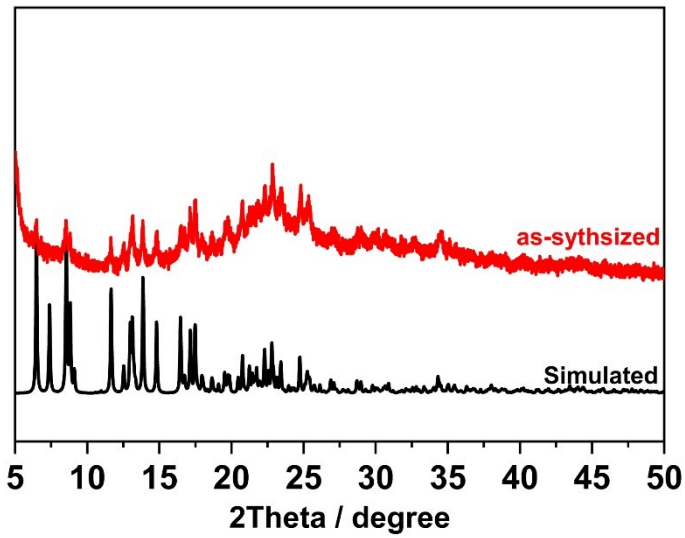

Fig. S15 Simulated and as-synthesized PXRD patterns of **CUST-713**.

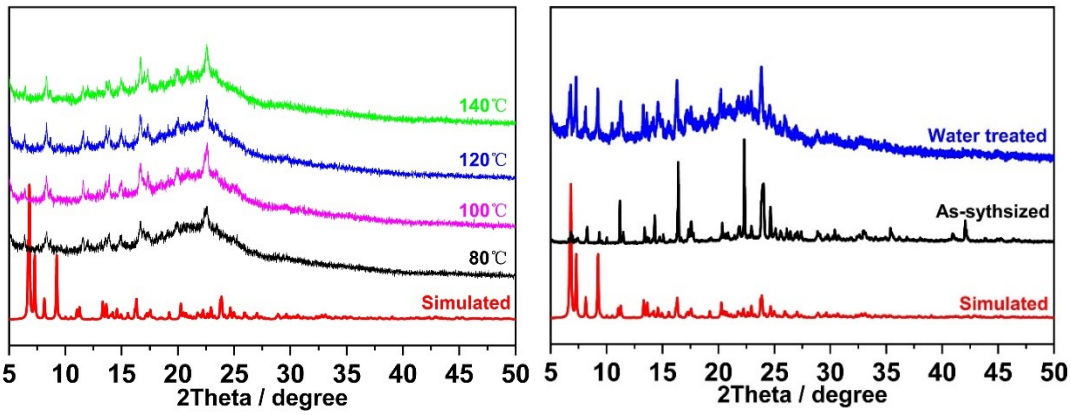

Fig. S16 PXRD patterns of **CUST-711** with different temperatures and PXRD patterns of samples soaked in water after high temperature treatment.

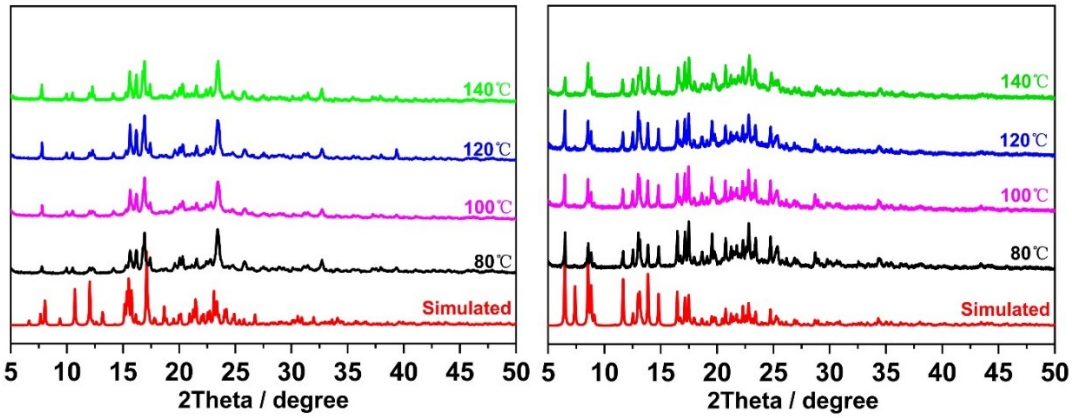

Fig. S17 PXRD patterns of **CUST-712** and **CUST-713**with different temperatures.

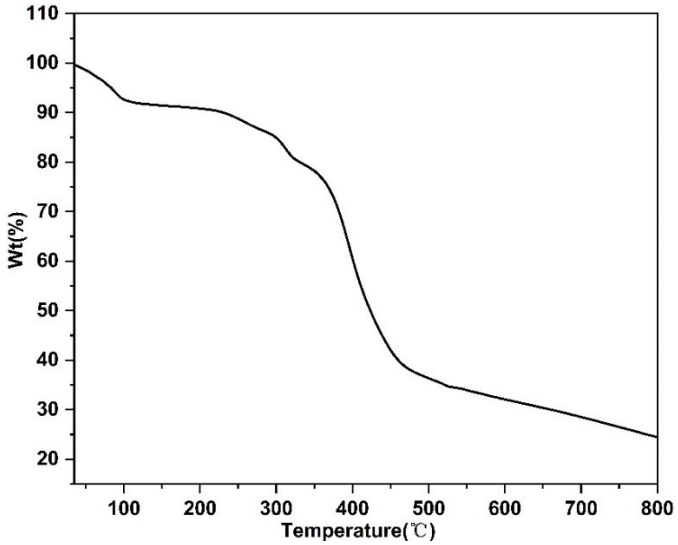

Fig. S18 TGA curve of **CUST-711.**

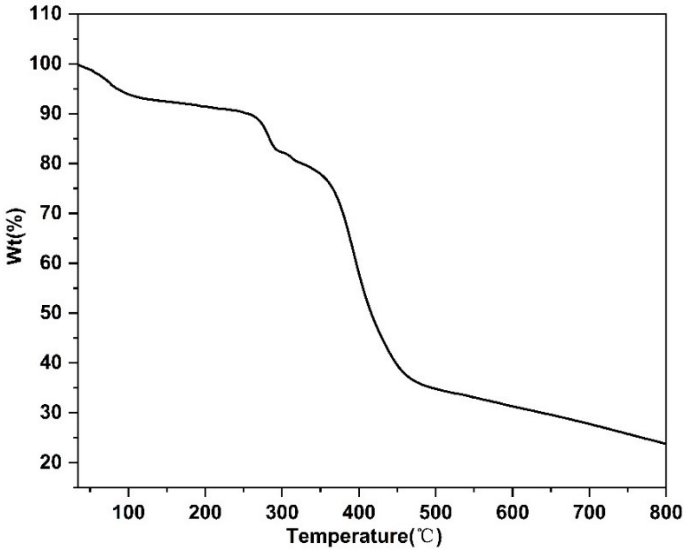

Fig. S19 TGA curve of **CUST-712.**

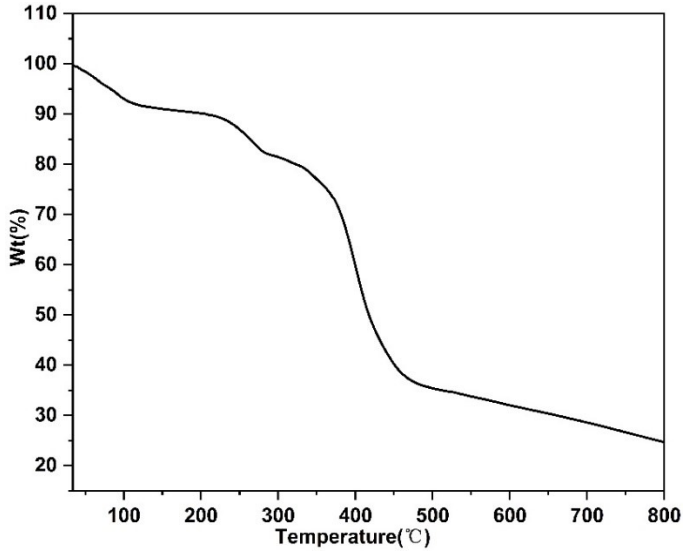

Fig. S20 TGA curve of **CUST-713.**

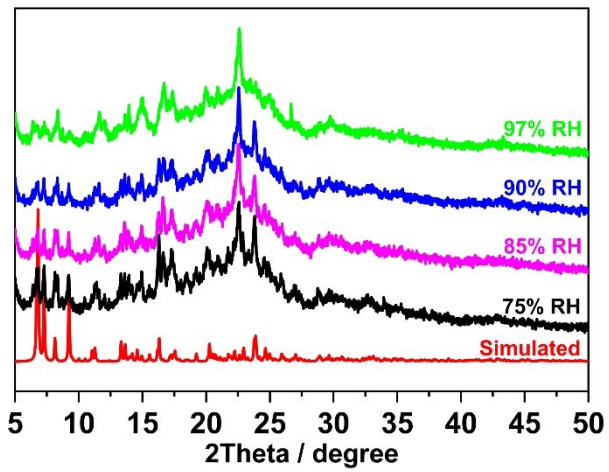

Fig. S21 PXRD patterns of **CUST-711** and **CUST-711** with different relative humidities.

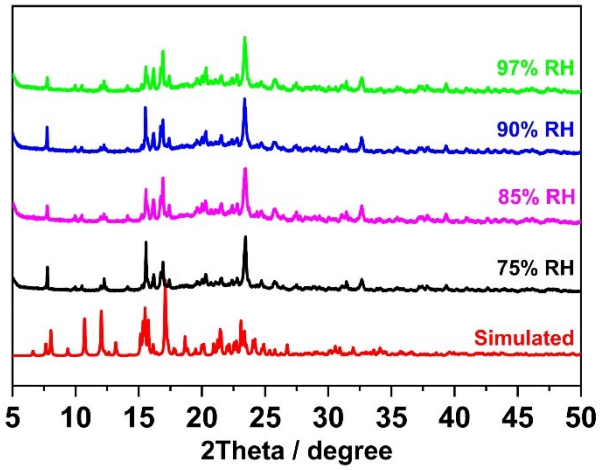

Fig. S22 PXRD patterns of **CUST-712** and **CUST-712** with different relative humidities.

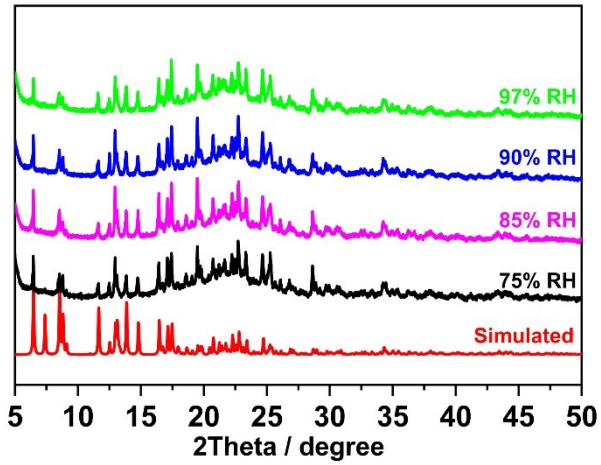

Fig. S23 PXRD patterns of **CUST-713** and **CUST-713** with different relative humidities.

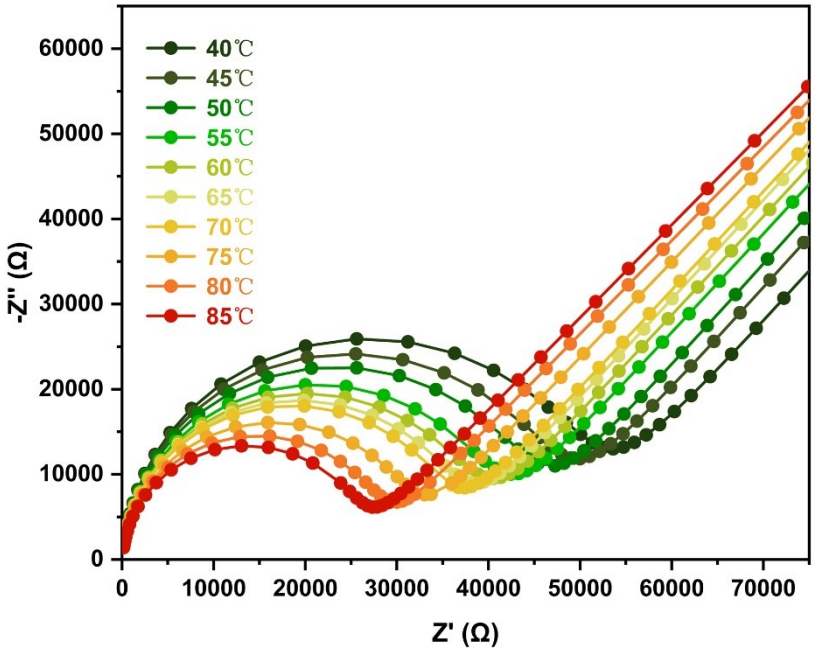

Fig. S24 Nyquist plots of **CUST-711** at 97% RH and different temperatures of 40–85 °C.

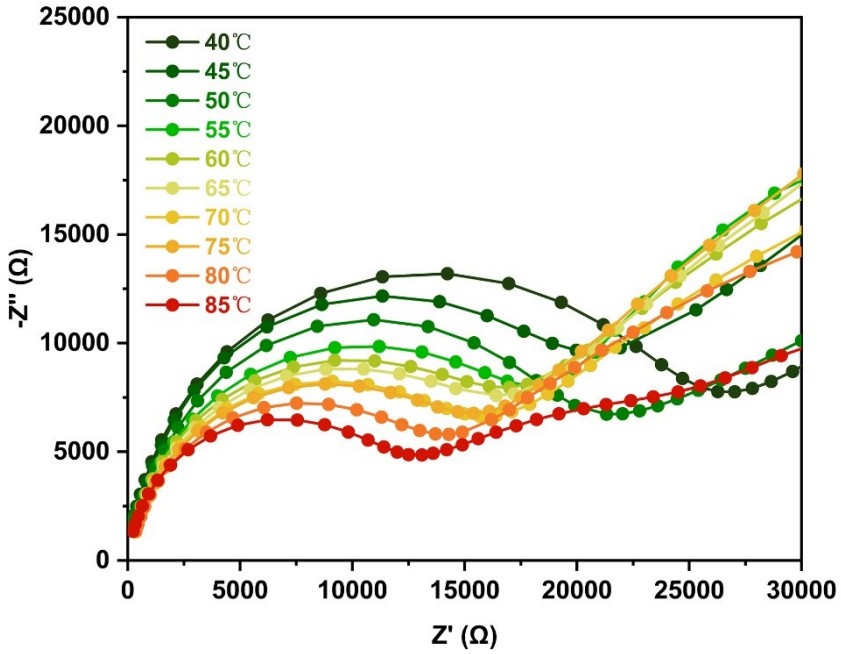

Fig. S25 Nyquist plots of **CUST-713** at 97% RH and different temperatures of 40–85 °C.

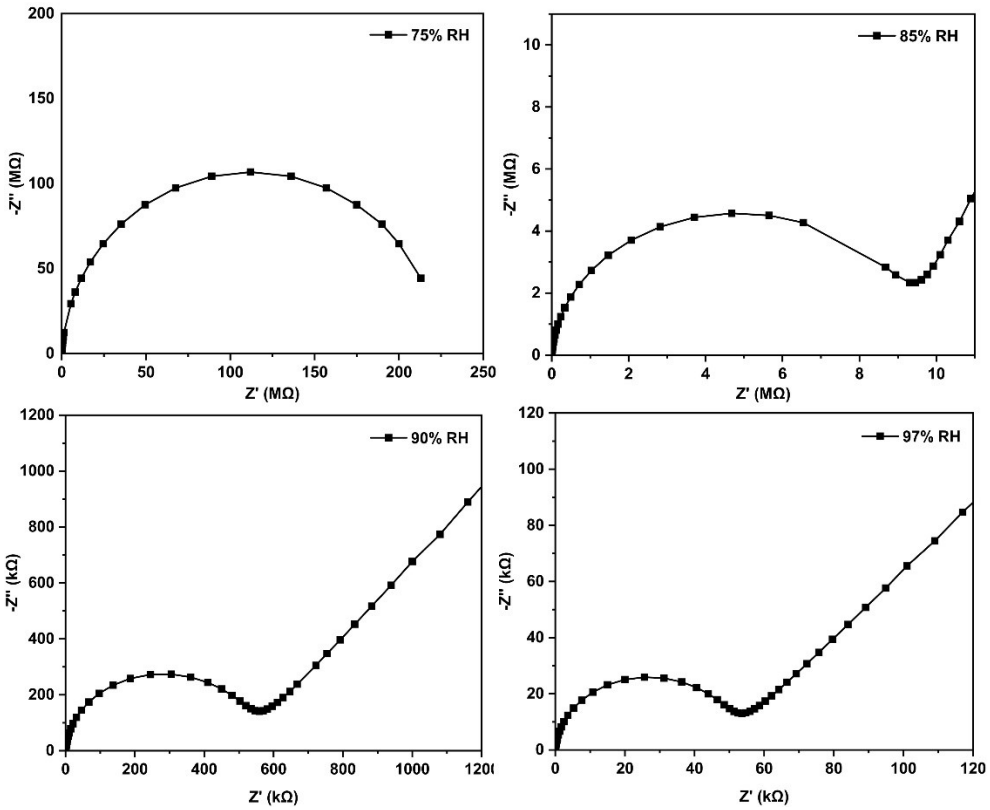

Fig. S26 Nyquist plots of **CUST-711** at 40 °C and different relative humidity of 75%-97% RH.

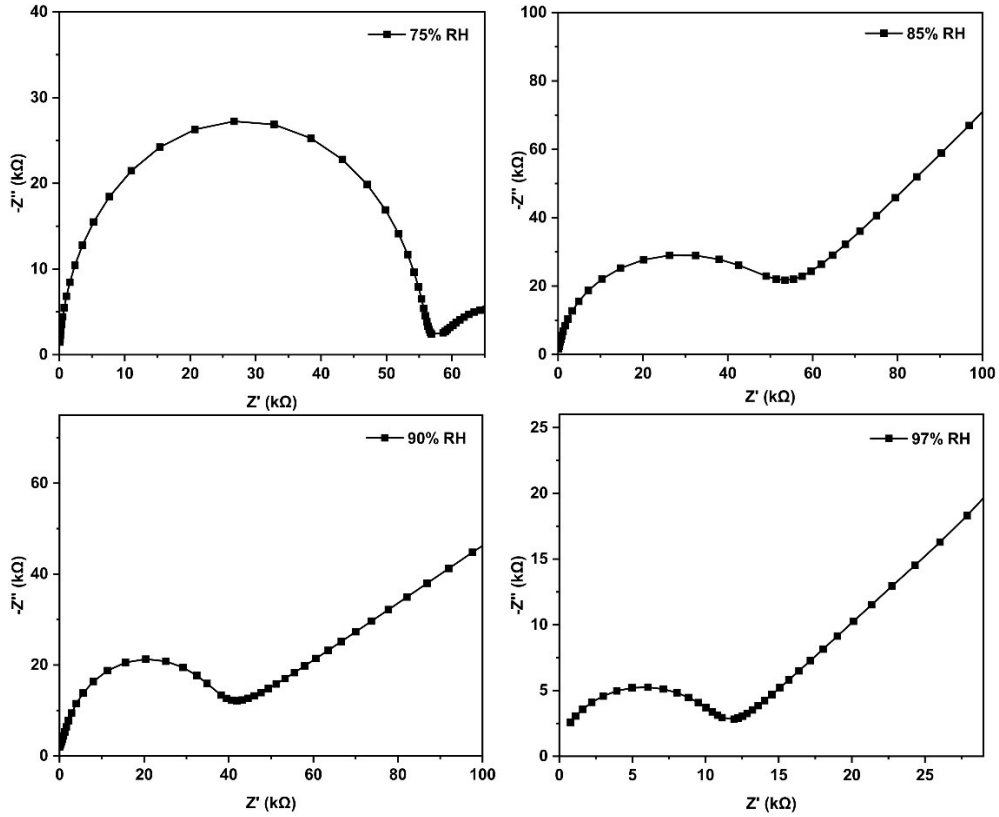

Fig. S27 Nyquist plots of **CUST-712** at 40 °C and different relative humidity of 75%-97% RH.

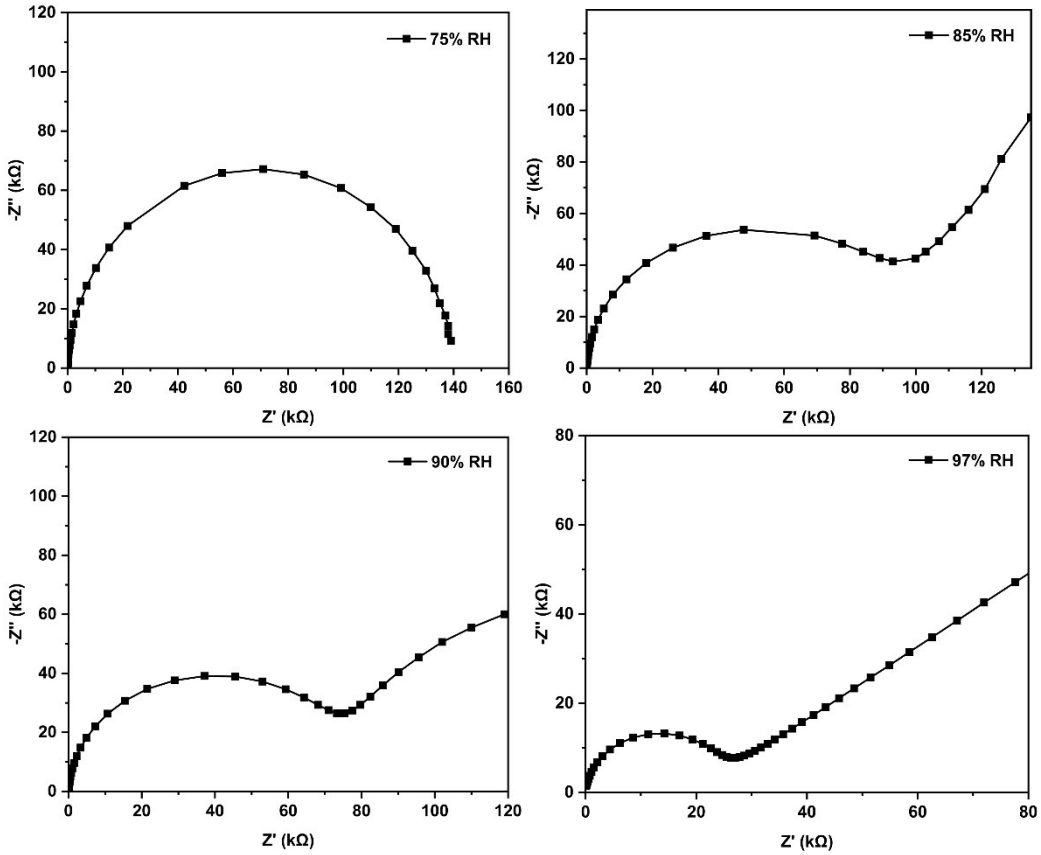

Fig. S28 Nyquist plots of **CUST-713** at 40 °C and different relative humidity of 75%-97%

RH.

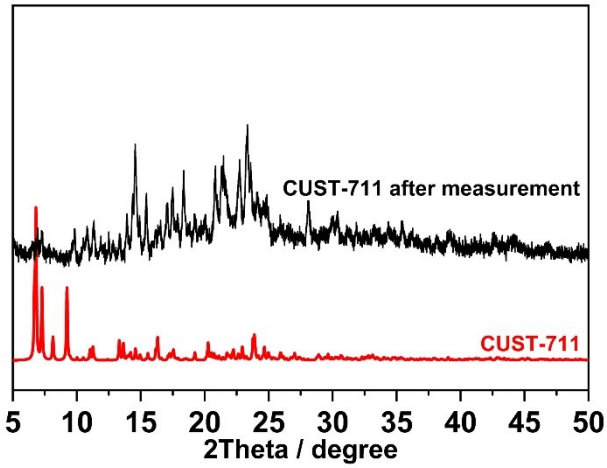

Fig. S29 PXRD patterns of **CUST-711** after impedance analysis.

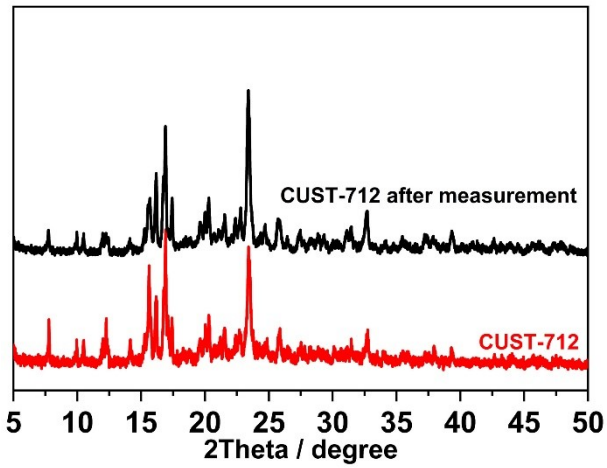

Fig. S30 PXRD patterns of **CUST-712** after impedance analysis.

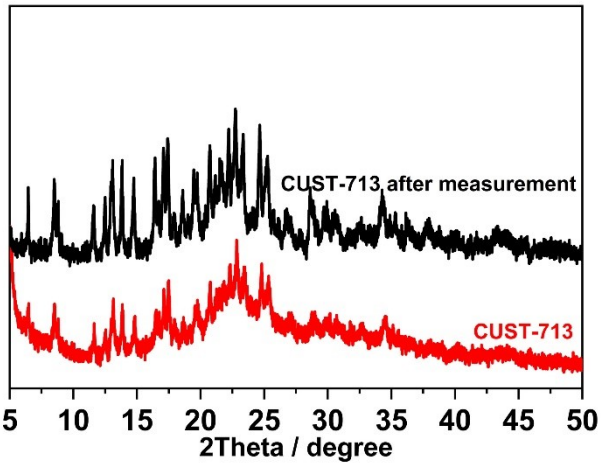

Fig. S31 PXRD patterns of **CUST-713** after impedance analysis.

References

1 Z.-B. Wang, H.-F. Zhu, M. Zhao, Y.-Z. Li, T.-a. Okamura, W.-Y. Sun, H.-L. Chen and N. Ueyama, *Cryst. Growth Des.*, 2006, **6**,1420-1427.

2 D. Bardelang, K. A. Udachin, D. M. Leek, J. C. Margeson, G. Chan, C. I. Ratcliffe and J. A. Ripmeester, *Cryst. Growth Des.*, 2011, **11**, 5598-5614.